GCA TECHNICAL REPORT
60-3-N

ELECTRON PRODUCTION IN THE E AND F REGIONS

DR. KENICHI WATANABE

NATIONAL AERONAUTICS AND SPACE ADMINISTRATION
GODDARD SPACE FLIGHT CENTER
WASHINGTON, D.C.

DECEMBER 1960

GEOPHYSICS CORPORATION OF AMERICA
BEDFORD, MASSACHUSETTS

GCA Technical Report
60-3-N

ELECTRON PRODUCTION IN THE E AND F REGIONS

Dr. Kenichi Watanabe

NATIONAL AERONAUTICS AND SPACE ADMINISTRATION
Goddard Space Flight Center
Washington, D.C.

December 1960

GEOPHYSICS CORPORATION OF AMERICA
Bedford, Massachusetts

TABLE OF CONTENTS

LIST OF ILLUSTRATIONS

ABSTRACT

Photoionization rates in the E and F regions were computed on the basis of recent data on solar ultraviolet flux, reference atmosphere, and absorption cross-sections. These rates were found to be ten to hundred times larger than previous values but in harmony with the requisite rates deduced from radio propagation studies.

Our results show that the E region ionization is mainly due to radiation in the spectral range 900-1027 A and less than 5 percent to soft X-rays. The base of the E region, 95-105 km, is controlled largely by Lyman beta. The Lyman continuum (911-850 A), the C III line at 977 A, and other lines in the range 900-1000 A contribute to the upper E region.

The electron production in the F region is primarily due to ultraviolet radiation in the range 100-900 A. At sunrise the maximum ionization rate is at about 300 km, roughly coinciding with the peak of nighttime electron density but the maximum descends to about 150 km for zenith sun. The F_2 peak is apparently due to the combined result of the daytime enhancement of electron density and the slow recombination. The F_1 ledge follows the maximum of ionization and descends to 150 km as the solar zenith angle goes from 90 to 0^o. Electron densities computed with the aid of observed recombination coefficients are in good agreement with values obtained from rockets and satellites.

I. INTRODUCTION. Although some thousands of papers have discussed the formation, nature, and behavior of the E and F regions of the ionosphere, as yet we do not have a quantitative and generally acceptable description of the origin of these regions. A study of even a few review articles shows that our knowledge of the basic data on solar radiation flux, concentration of atmospheric constituents at various altitudes, and photoionization cross section as well as total cross section of each constituent at various wavelengths has been very inadequate, so that an investigator had to resort to assumptions or rough estimates in order to arrive at conclusions. For example, some investigators have ascribed the ionization in the E region to solar x-rays, while others have given preference to the photoionization of O_2 by solar ultraviolet radiation in the spectral range 900-1027 A. A decision can be made readily as soon as the flux in the relevant spectral ranges is quantitatively established. In other words, we have too many theories on the origin of the ionosphere, and now the problem appears to be one of determining the relative importance of several possible mechanisms on the basis of new data.

In the past several years, major advances have been made in the measurements of the necessary data, particularly by means of rockets and satellites. Although some of the data are not sufficiently precise, one can make a more detailed and quantitative study of the photoionization rates than it was previously possible. Nicolet and Aiken [1] have already made a rather thorough study of the D region

which involves radiation in the spectral ranges 1100-1340 A and below 10 A. In the present study, we are primarily concerned with the E and F regions which involve a different spectral range, 10-1100 A.

Before we calculate the ion production rates we must make some selections from the three categories of basic data because these data are not firmly established, and in some cases they disagree by more than an order of magnitude. Despite the uncertainties inherent in such selections, there exist some reliable observations which can guide us towards a fairly consistent set of parameters.

II. SOLAR ULTRAVIOLET FLUX. The major observational gap in the solar spectrum, 100-1100 A, has been largely closed during the past two years by the work of Hinteregger et al.[2], Rense et al.[3], and Tousey et al.[4]. Their results show that the solar spectrum in this region is quite different from all previous estimates or assumed spectra, and for the first time, calculations of ion-production rates for the E and F regions can be based on realistic values of solar flux.

The solar spectrum in the range 100-1100 A is very complex; there are many emission lines both weak and strong and there are also emission continua such as the Lyman continuum of hydrogen which provides a significant amount of energy. Therefore, the ion-production rates must be calculated in terms of solar flux at many wavelengths rather than in terms of a single continuum such as a blackbody curve or a few emission lines.

According to the results of these observers, the incident solar ultraviolet flux in the spectral region 100-1100 A is much larger than an earlier estimate, 0.1 erg $cm^{-2}sec^{-1}$ by Havens et al.[5] For example, according to Tousey's preliminary photographic data [4] the intensity of Lyman beta (1025.7 A) alone is 0.06 erg $cm^{-2}sec^{-1}$; Hinteregger using a photoelectric technique has observed a combined flux of 2.8 ergs $cm^{-2}sec^{-1}$ in the range 60-1000 A at an altitude of 210 km; while Reese and Rense [3] extrapolated as much as 15 ergs $cm^{-2}sec^{-1}$ for the He II line at 304 A from photographs obtained at about 200 km.

In the present study, the magnitude of the minimum ion production rates was used as a guide to select the solar flux from the available data. Bates [6] has already pointed out that the flux used by Havens, Friedman, and Hulburt [5] lead to insufficient ionization rates. On the other hand, the flux of 15 ergs $cm^{-2}sec^{-1}$ for the He II line [3] gives too high rates of ionization when the flux of other emission lines and continua is proportionately included. Some preliminary calculations for the altitude range 90-400 km indicated that the data by Hinteregger [2] and Tousey [4] lead to reasonable ionization rates.

The solar flux shown in Table 1 was used in our computation of photoionization rates. For the spectral range 900-1027 A, the listed values lie between those by Tousey and by Hinteregger, the latter being higher. For the range 100-911 A, the selected flux is about 30 percent higher than the flux observed by Hinteregger et al[2] at 210 km but is about one-third their extrapolated value. Such an

Table 1

Solar flux, I_o in 10^8 photons cm^{-2} sec^{-1}, for the spectral range 1027-10 A at normal incidence outside of Earth's atmosphere. The I_o's of weak lines and continuum are lumped together for each interval, while the prominent lines are listed separately.

λ (in A)		I_o	λ (in A)		I_o
1025.7	Ly β	35	629.7	O V	10
1011	lines	2.5	610,625	MgX	10
1000-1027		3.5	584.3	HeI	15
989.8	N III	10	554	O IV	2
977.0	C III	29	537	HeI	4
972.5	Ly γ	9.7	520	Si XII	9
949.7	Ly δ	4.0	500-650		60
937.8	Ly ϵ	2.3	499	Si XII	5
934,944	S VI	1.9	303.8	He II	68
930-1000		6.7	300-500		63
911-930		13.7	250-300		21
850-911		134	170-250		25
834	O II,III	6	100-170		4.5
800-850		21	60-100		4.2
788,790	O IV	5	40-60		0.5
770,780	Ne III	5	20-40		0.15
650-800		71	10-20		0.015

extrapolation, of course, depends on the choice of reference atmosphere and absorption cross sections; in the present case, the correction is much less, as discussed below in Section V. For the region 10-100 A, the total flux given in Table 1 is a little higher than the 0.1 erg cm^{-2} sec^{-1} obtained by Byram et al.[7] who matched the responses of three photon counters to a single coronal temperature. Some values in Table 1 are our estimates based on visual comparison of emission lines in the solar spectrum[4]. The uncertainty in the total flux is probably no more than a factor of two, since Hinteregger et al.[2] have used a photoelectric technique which is very amenable to energy calibration and quite insensitive to scattered light.

The longest wavelength in Table 1 corresponds to the first ionization potential of O_2 but it should be noted that photons of longer wavelengths can ionize O_2 in the excited state. For example, at a temperature of 1000°K about 10 percent of O_2 molecules are in the first vibrational level; hence, radiation of wavelengths up to 1043 A can ionize these molecules. In the altitude region above about 150 km, the solar O VI emission lines at 1032 A and 1038 A with intensities (6×10^9 photon $cm^{-2}sec^{-1}$) comparable to that of Lyman beta can produce some ionization.

III. COMPOSITION AND NUMBER DENSITIES. Atmospheric densities in the F region are now fairly well known from satellite observations. These densities are about one to two orders of magnitude larger than estimates based on extrapolation of earlier rocket data measured at altitudes below 200 km; in particular, the large discrepancy at about

200 km seems to have been removed by recent rocket and satellite data (8 through 11).

The curve of atmospheric density shown in Fig. 1 was used in the present study. For densities in the region 100-200 km, the results of Soviet rocket measurements [8] rather than those by Horowitz and LaGow [12] have been used because the former are more consistent with satellite data at about 200 km. For the region 170-250 km, our curve is closer to the satellite values by Champion and Minzner [9] than those by Schilling and Sterne [10]; this choice makes our curve nearly coincide with the Soviet rocket data [8]. For the region 250-400 km our curve falls about 20 percent below the results of Mikhnevich et al. [8]; however, our curve (not shown in Fig. 1) falls on the points at 450 and 750 km given by Siry [11]. Thus, our reference curve does not depart very much from most of the recent data, and its uncertainty is probably no more than a factor of two over most of the range.

One of the serious deficiencies in our knowledge is the atmospheric composition in the E and F regions which is required to calculate the number densities of major constituents. Although the composition of ionic particles has been measured with mass spectrometers by American and Soviet investigators, we lack data on neutral constituents which have much larger number densities. For example, we have no experimental data on the dissociation of N_2 and the degree of mixing and diffusion in the region above 150 km.

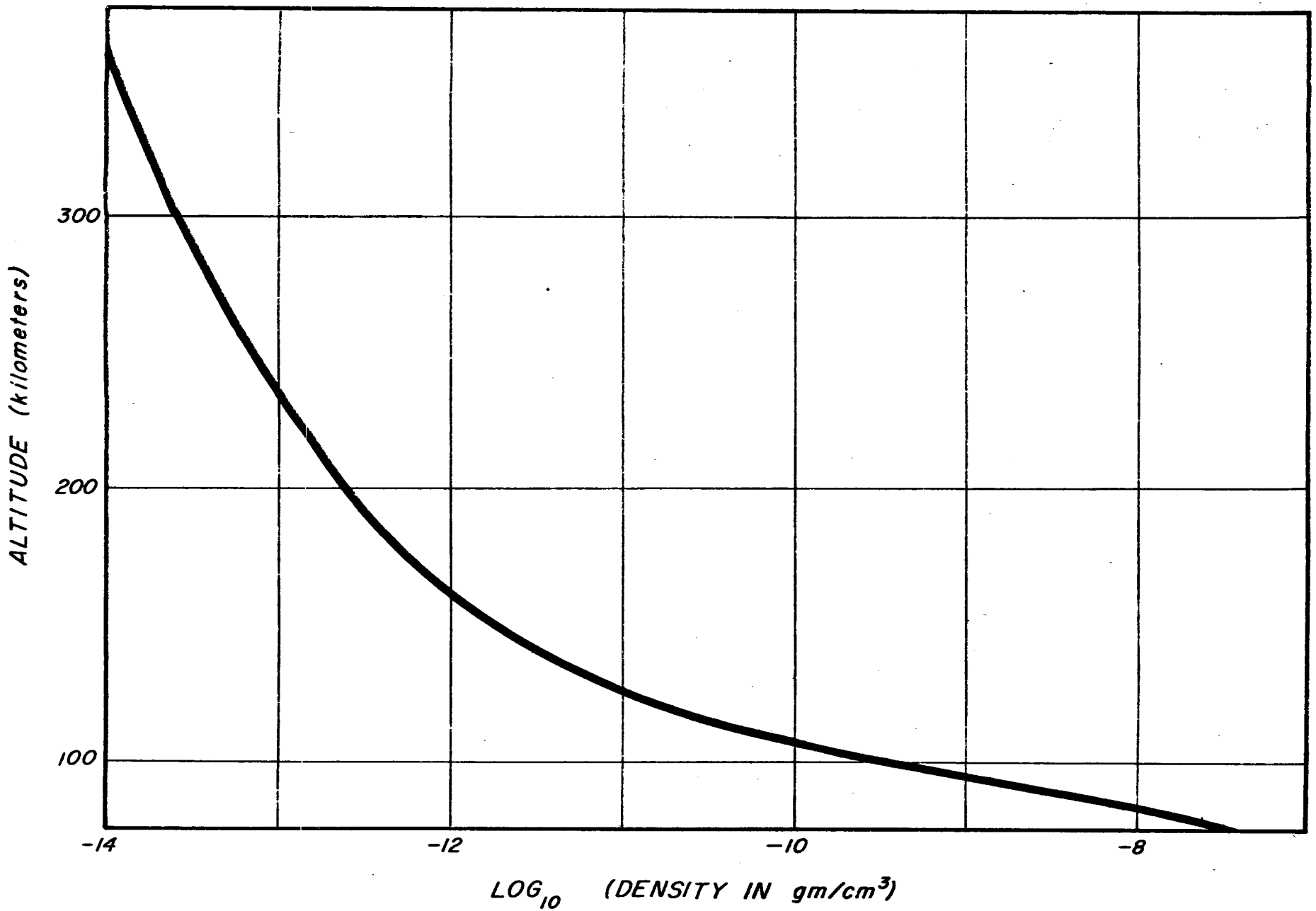

Figure 1 . Atmospheric Density Versus Altitude

Some theoretical calculations [13,14] have indicated that N_2 is nearly completely dissociated in the region above 200 km; the actual case seems to be quite the contrary. For example, the absorption of solar Lyman gamma in Tousey's photographs [4] suggests that there are considerable amounts of N_2 molecules above 200 km. Istomin [15] has reported that O_2^+ and N_2^+ ions are present up to 500 km and the amount of N^+ in the region 200-400 km appears to be small compared to that of O^+. Recently, Nicolet [16] has presented curves showing that NO and atomic nitrogen are minor constituents in the region above 100 km up to about 400 km.

Byram, Chubb, and Friedman [17] have reported that rocket measurements give 45 percent dissociation of O_2 at 110 km and 67 percent at 130 km. Bates and Nicolet [18], however, have used somewhat lower values: 24 percent at 150 km and 65 percent at 300 km.

In view of these uncertainties, we have considered several models of atmospheric composition based on different amounts of O_2 and N_2 dissociation and diffusion. These models were tested against solar spectra [2,3,4] at various altitudes. Several emission lines in the region 1000-1500 A were used to check O_2 absorption in the altitude range 100-150 km and the Lyman gamma line to check N_2 absorption at higher altitudes. Such test did not lead to a sharp discrimination of the several models, but a model similar to that used by Bates and Nicolet [18] appeared to be the most satisfactory. This model assumes a relatively low amount of O_2 dissociation as mentioned above, negligible amount of N_2 dissociation up to 400 km, and increasing amount of diffusion above 200 km,

making the number density of O comparable to that of N_2 at altitudes above 300 km.

The number densities n of O, O_2, and N_2 which were used in the present study are listed in Table 2 . These densities are on the whole somewhat lower than those by Bates and Nicolet [18] since we adopted somewhat lower atmospheric densities.

The transmission of solar ultraviolet radiation can be calculated from the layer thickness L which is defined by

$$L = \frac{1}{n_o} \int n \, ds \qquad (1)$$

where n is the number density of a given constituent, n_o is Loschmidt's number, s = path length in cm, and L = layer thickness in cm (at STP). The values computed by numerical integration for O, O_2, and N_2 at vertical incidence are listed in Table 2.

L for other zenith angles Z were also computed. For Z up to about 80^o, the factor sec Z dl may be used in place of ds in Eq. 1, the error introduced being smaller than other uncertainties.

Emphasis should be given to the fact that the change of L with increasing Z depends roughly on the "scale height." This dependence appears to be very important in the formation of the F region. Since the number density decreases rather rapidly with height, we can represent its distribution approximately by

$$n = n_h \exp\left(-\frac{x}{H}\right) \qquad (2)$$

Table 2

Number density n (in particles/cm^3) and layer thickness L (in cm reduced to STP) at various altitudes h (in km)

h	n			L		
	O	O_2	N_2	O	O_2	N_2
90	7.1×10^{11}	1.16×10^{13}	4.2×10^{13}	3.8×10^{-2}	2.14×10^{-1}	8.2×10^{-1}
95	7.3	4.2×10^{12}	1.62	2.36	8.4×10^{-2}	3.3
100	4.2	1.55	6.2×10^{12}	1.30	3.6	1.46
105	2.3	6.5×10^{11}	2.7	7.2×10^{-3}	1.63	7.0×10^{-2}
110	1.13	2.8	1.18	4.1	8.3×10^{-3}	3.7
115	5.8×10^{10}	1.31	5.7×10^{11}	2.64	4.7	2.14
120	3.3	7.1×10^{10}	3.1	1.84	2.96	1.36
130	1.29	2.4	1.09	1.07	1.41	6.8×10^{-3}
140	6.6×10^{9}	1.10	5.1×10^{10}	7.4×10^{-4}	8.3×10^{-4}	4.0
150	3.8	5.7×10^{9}	2.7	5.6	5.2	2.63
160	2.5	3.3	1.62	4.4	3.6	1.85
170	1.75	2.1	1.07	3.7	2.62	1.36
180	1.28	1.42	7.3×10^{9}	3.1	1.97	1.03
200	8.1×10^{8}	7.5×10^{8}	4.0	2.37	1.22	6.2×10^{-4}
220	5.8	4.6	2.4	1.87	7.9×10^{-5}	4.0
250	3.7	2.3	1.12	1.35	4.3	2.1
300	1.98	8.1×10^{7}	3.8×10^{8}	8.4×10^{-5}	1.63	8.4×10^{-5}
350	1.20	3.2	1.57	5.4	6.5×10^{-6}	3.8
400	7.9×10^{7}	1.32	7.2×10^{7}	3.6	2.6	1.81
500	3.6	1.9×10^{6}	1.6	1.6	4×10^{-7}	4×10^{-6}

where n_h = number density of a given constituent at a given height h, x = height above h, and H is taken as a constant (height constant) but not in general equal to the conventional "scale height." In our model at 300 km, H is about 60 km for O_2 and 120 km for O. Using Eqs. 1 and 2, letting dx = ds, and taking zero and infinity as limits, we obtain

$$L = \frac{n_h H}{n_o} \tag{3}$$

For $Z = 90^o$, ds is replaced by the approximate quantity $(R/2x)^{\frac{1}{2}}\, dx$ where R is the distance to the Earth's center from h; then integral (1) becomes

$$L' = \frac{n_h}{n_o} \int_0^\infty (R/2x)^{\frac{1}{2}} \exp\left(-\frac{x}{H}\right) dx = (R\pi H/2)^{\frac{1}{2}} \tag{4}$$

The ratio of the L's is

$$L'/L = (R\pi/2H)^{\frac{1}{2}} \tag{5}$$

Letting R = 6600 km, we have

$$L'/L \sim 100/(H)^{\frac{1}{2}} \tag{6}$$

where H is now in km. At 100 km, H is less than 10 km for N_2, but at 300 km, it is one order of magnitude larger. Thus, the change of layer thickness as Z goes from 0^o to 90^o is significantly different for the E and the F regions.

IV. ABSORPTION AND PHOTOIONIZATION CROSS SECTION

Our knowledge of the absorption cross section, although incomplete, appears

to be adequate for the present purpose, since our computations involve many wavelengths and inaccuracies at a few wavelengths have only small effects on the total rates. Furthermore, available data include many lines found in the solar spectrum. Published data on absorption cross sections have been reviewed[19] and some recommended values for O_2 and N_2 are given in the Appendix. Dalgarno [20] has presented new sets of recommended values for O atom from its ionization threshold to 0.1 A (see Appendix).

The wavelengths corresponding to the ionization threshold of O_2, O, and N_2 are, respectively, 1027, 911, and 796 A. Calculations of photoionization rates require both the total absorption and the photoionization cross sections of these constituents, since part of the solar ultrviolet flux in the region below 1027 A is removed by absorption processes not leading to ion production. For example, solar Lyman gamma (972.5 A) can ionize O_2 molecules but is almost entirely absorbed by N_2 molecules at altitudes above 200 km and makes negligible contribution to the ionosphere. As pointed out by Kato [21], part of the solar Lyman beta is absorbed by atomic oxygen, but the amount appears to be small [22] due to the fact that Lyman beta is broadened as in the case of Lyman alpha [23].

Atmospheric absorption in the spectral range 800-1100 A which is important to the E region is essentially controlled by O_2 and N_2. For O_2, both the absorption and and photoionization cross sections have been measured by Watanabe and Marmo [24] at many wavelengths.

But for N_2, published data are meager and poor due to the complexity of the N_2 absorption spectrum. Absorption coefficients vary from almost zero to as high as 7600 cm^{-1} in this region. Some data by Itamoto et al.[25] were used in the present study.

For the spectral region 100-800 A which is important to the F region, available data are rather meager; however, the spread in the absorption coefficient is comparatively small owing to the fact that continous absorption sets in for all major constituents. The spread is probably from 100 cm^{-1} to 1000 cm^{-1}. For example, at 584 A, the absorption coefficients of O_2, N_2, and O are, respectively, 540, 520, and 350 cm^{-1}, and at 304 A, respectively, 300, 160, and 250 cm^{-1}. The photoionization yield is also uniformly high, nearly 100 percent in most cases. Thus, errors in the cross section appear to be less serious than errors in atmospheric composition.

V. PENETRATION OF SOLAR ULTRAVIOLET. The solar ultraviolet flux available at each altitude is calculated by means of the equation

$$I = I_o \exp\left(-\sum k_i L_i\right) \tag{7}$$

where I_o and I are the incident and transmitted flux for a given wave length, k_i = absorption coefficient of each constituent, and L_i is the layer thickness for each constituent as given in Table 2 . Transmission, T in percent, is defined by

$$T = 100\ (I/I_o) \tag{8}$$

The results for some of the wavelength at vertical incidence are shown in Fig. 2. Similar calculations were made for other solar zenith angles: $Z = 70.5^{\circ}$, 84.3° and 90°.

Fig. 2 combined with other results not drawn in, show that for $Z = 0^{\circ}$, radiation of wavelengths 800-1027 A is absorbed mainly in the altitude range 100-150 km (E region), while radiation in the range 100-800 A is absorbed mostly at altitudes 140-200 km or the lower F region. Only a small portion of the solar ultraviolet is absorbed in the region above 200 km at $Z = 0^{\circ}$ since the absorption coefficient of the predominant gases are less than 1000 cm^{-1} at most wavelengths. An interesting exception is Lyman gamma; at its wavelength, k = 7600 cm^{-1} for N_2 and about 1000 cm^{-1} for O_2. Our results for the depth of penetration are somewhat higher than our previous estimates [19] because the new atmospheric densities above 150 km are much higher than pre-satellite data.

The results of our calculations were checked against photographs of solar spectrum [4]. For example, the solar C III line at 977 A penetrates to about 110 km and Lyman gamma down to 200 km, in agreement with rocket observations; no serious discrepancies were found but the available spectra are still insufficient to permit quantitative comparisons. It should be borne in mind, however, that laboratory absorption coefficients may not be directly applicable if the solar emission line is much broader than the corresponding line used in the laboratory. This appears to be the case in Lyman gamma, which may be detectable at altitudes below 200 km.

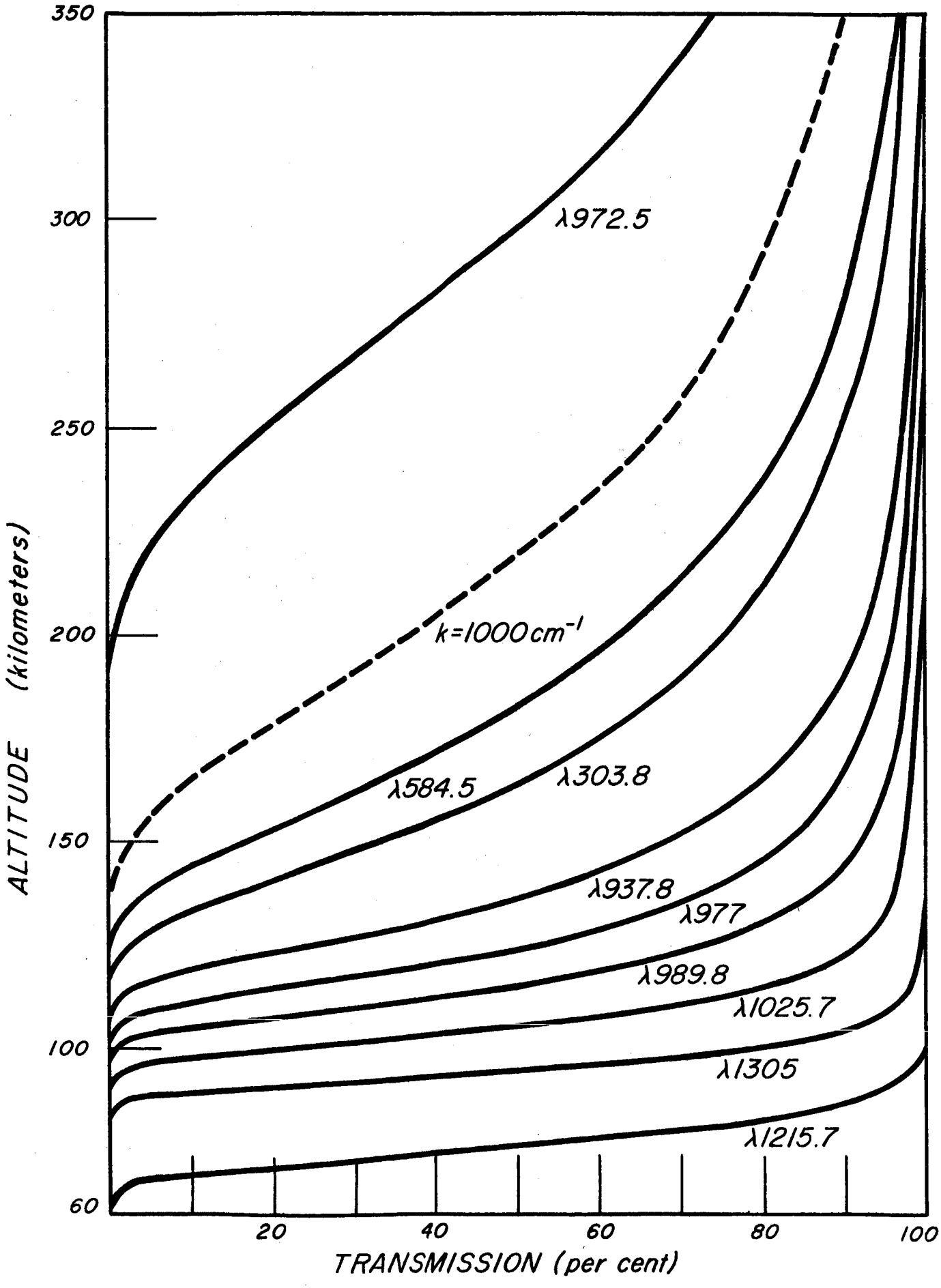

Figure 2 Transmission at Normal Incidence Versus Altitude for Several Solar UV Emission Lines. Broken curve is for air with effective k = 1000 cm^{-1}.

Fig. 2 is also consistent with the rapid change in the scale height at about 120-170 km (see Fig. 1). Since the maximum rate of absorption of most radiation in the range 100-1100 A occur in this altitude region, there should be considerable heating here.

Transmission curves similar to Fig. 2 have been presented for the x-rays by Friedman[26].

VI. PHOTOIONIZATION RATES. Mathematical expressions for the rate of ion-pair production in the atmosphere under the action of solar radiation have been derived by Chapman[27,28,29] and others[30,31] using various assumptions. The original Chapman theory[27] assumes monochromatic radiation, isothermal atmosphere, and a single gas constituent. The theory has been extended to include other assumptions such as varying scale height[30,31] and band absorption[28]. These derived expressions serve as valuable theoretical background but cannot be applied readily to the present conditions (varying composition, varying scale height, complex solar spectrum and many absorption and photoionization cross sections). Therefore, we have used numerical summation of the various components as was done for the layer thickness L.

The photoionization rate p in ion-pair cm^{-3} sec^{-1} at a given altitude was computed according to the expression

$$p = \sum_{\lambda} I_{\lambda} \left(\sum \sigma_i \; n_i \right) \qquad (9)$$

where I_λ is the ultraviolet flux for a given wavelength at the given altitude as derived by Eq. (3.7), σ_i = photoionization cross section of each

constituent at each wavelength, and n_i is the number density of each constituent at the given altitude.

It is of interest to subdivide the total p at each altitude into contributions from several spectral ranges: 911-1027 A which ionizes only O_2; 796-911 A which ionizes both O and O_2; 100-796 A which ionizes O, O_2, and N_2; and 10-100 A which is absorbed in the E region.

The photoionization rates were calculated for Z = 0°, 70.5°, 84.3°, and 90°; Figs. 3 and 4 show the rates for Z = 0° and Z = 84.3°, respectively. The broken curves represent the contributions of the four spectral ranges and the solid curve with two principal maxima, ϵ and $\varnothing$, gives the total rate. Fig. 4 also shows secondary maxima between ϵ and $\varnothing$. For Z = 0°, the lower maximum is at about 105 km (E region) and the higher maximum is at about 150 km (bottom of the F_1 region). For Z = 84.3°, the corresponding maxima have shifted to 120 and 260 km, respectively. The larger shift of the maximum $\varnothing$ is due to the large scale height in the region above 150 km as discussed in Section III and is the basis for the formation of the F_2 region.

The photoionization rates obtained in the present study are from 20 to 100 times larger than those computed by Havens, Friedman, and Hulburt [5] as shown in Table 3.

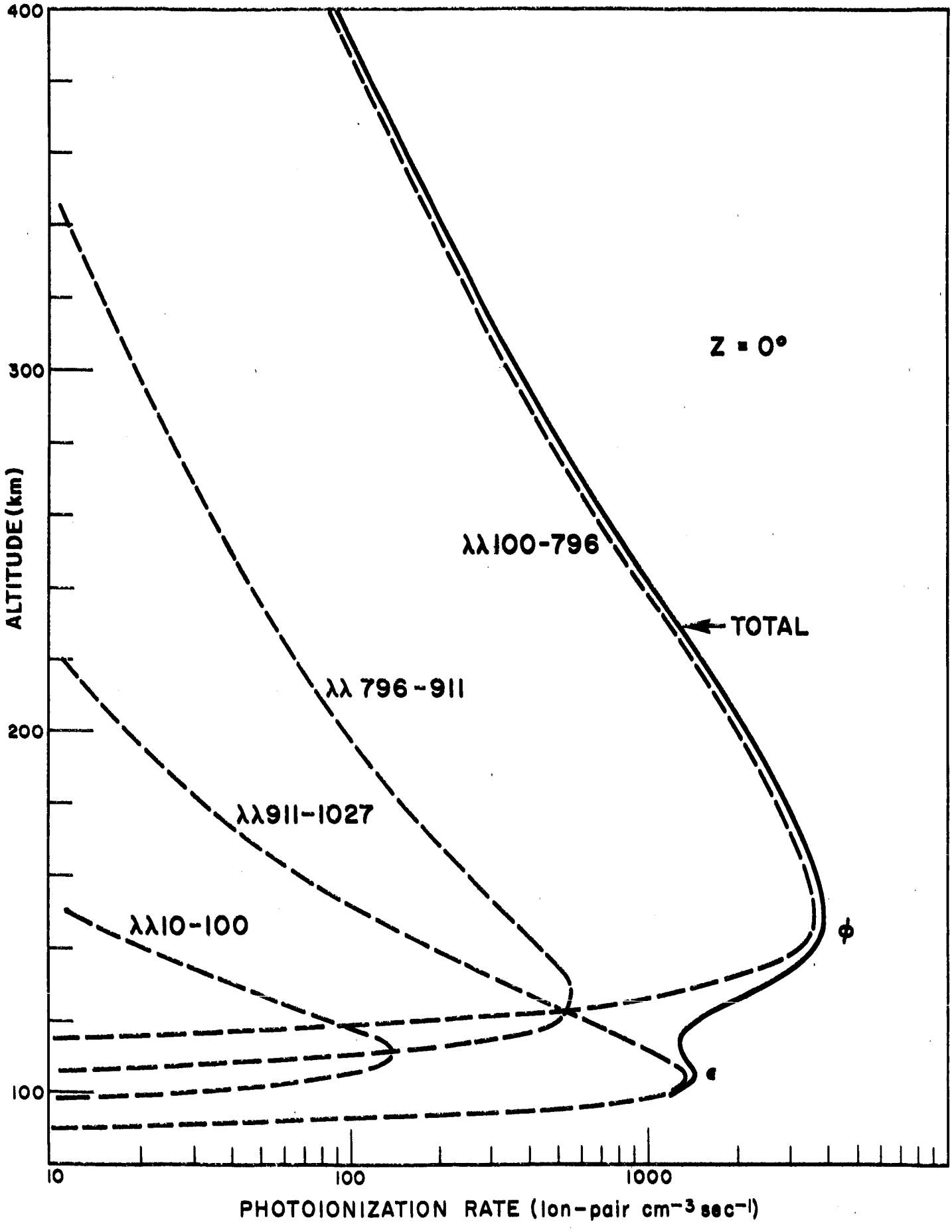

Figure 3. Photoionization Rate Versus Altitude for Normal Incidence. Broken curves give rates due to respective spectral ranges and solid curve total rate.

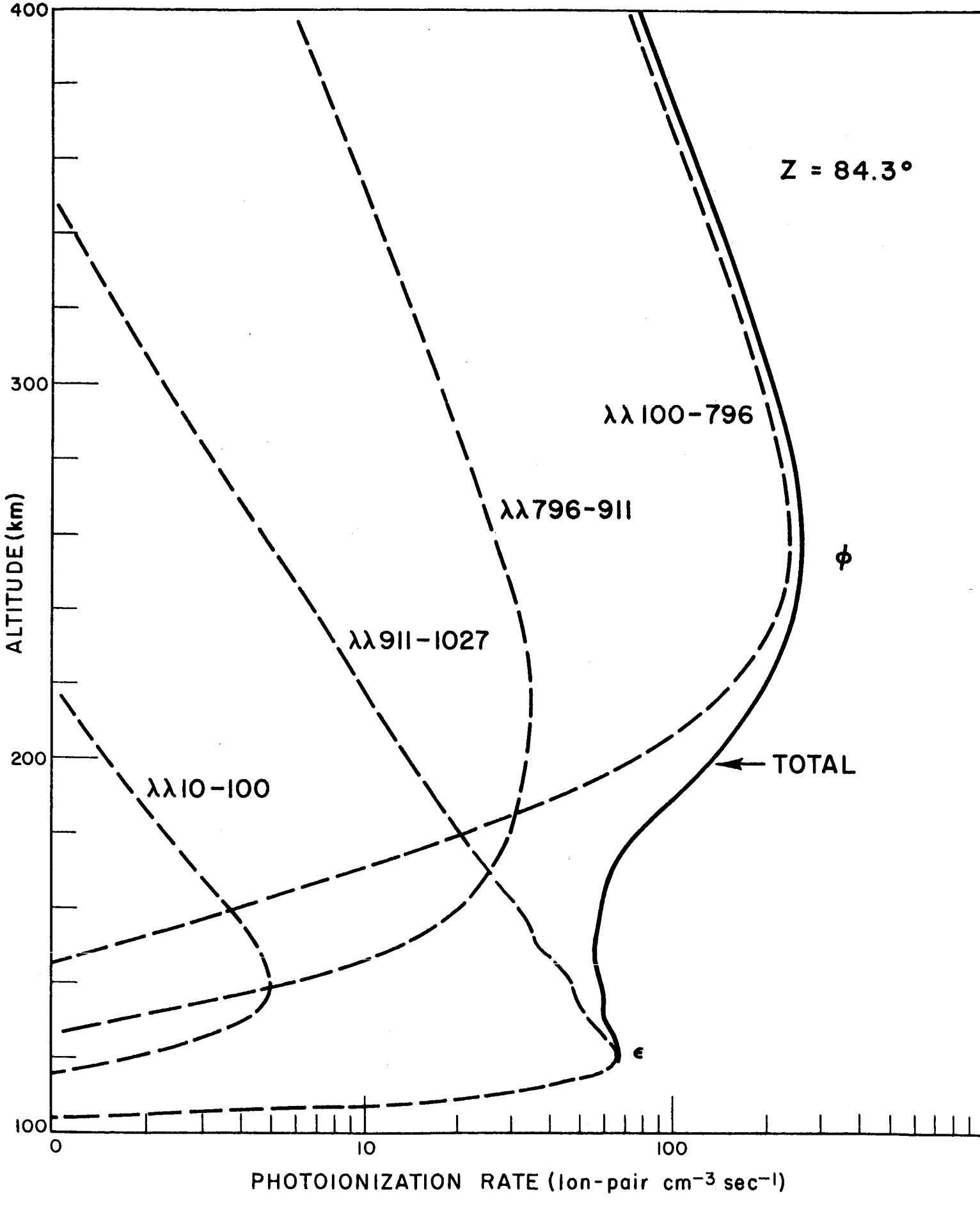

Figure 4. Photoionization Rate Versus Altitude for Solar Zenith Angle Equal to 84.3°

Table 3

PHOTOIONIZATION RATES (ION-PAIR CM^{-3} SEC^{-1})

Altitude (km)	150	200	250	300	350
Havens et al.	200	80	20	5	1.6
Present study $Z = 0^{o}$	3900	2200	890	380	180
$Z = 90^{o}$	17	36	125	155	115

The results obtained in the present study appear to be more in line with the requisite rates deduced from radio measurements. Johnson [32] found it necessary to increase the flux used by Havens et al. [5] by fifteen times in order to account for the high temperatures existing in the F region, and his indirect estimate of the flux for the He II line at 304 A is remarkably close to Hinteregger's [2] results.

The comparatively high ionization rates in the F region for $Z = 90^{o}$ show that ionization in this region is not negligible even during the twilight period. The ionization rate at about 300 km changes only by a factor of two throughout the day, but at 150 km the change is more than a factor of 10^{2}.

VII. FORMATION OF THE E REGION. The two competing theories for the formation of the E region are: (A) photoionization of O_2,

$$O_2 + h\nu\ (800\text{-}1027\ A) \rightarrow O_2^{+} + e \qquad (10)$$

as proposed by Wulf and Deming [33] and modified by Nicolet [34]; (b) general ionization of air by soft X-rays (10-100 A) suggested by Vegard [35] and Hulburt [36] in 1938. Many investigators [37-46] have made studies to determine the dominating process; however, these studies were based on rather incomplete data and often on incorrect assumptions such as blackbody solar spectrum. Most investigators[47] seem to favor the X-ray theory on the basis of intensity measurements by Byram, Chubb, and Friedman [7,26,40]; while Watanabe, Marmo, and Pressman [44] have given reasons for not rejecting the molecular oxygen theory.

The present study differs from earlier work in that we have used a flux (0.6 erg $cm^{-2}sec^{-1}$ or about $2.8x10^{10}$ photons $cm^{-2}sec^{-1}$) in the region 800-1027 A much higher than previous estimates (less than 0.001 erg $cm^{-2}sec^{-1}$ by Byram et al[40] and about 0.01 by Kamiyama[46]). The higher flux does not appear to be too high because it is about a factor of two lower than Hinteregger's value [2] at 210 km and the intensity of Lyman beta obtained by Tousey is quite consistent with the intensity of Lyman alpha. For the soft X-ray region, 10-100 A, we have used the value observed by Byram et al[7].

If the selected intensities are approximately correct, soft X-rays contribute less than 5 percent to the total ionization rate in the E region. Thus, the electron production of the normal E region is apparently due to photoionization of O_2 by the action of ultraviolet radiation in the range 800-1027 A. Some O^+ ions are formed in the upper E region by radiation in the spectral region 800-911 A which includes the strong Lyman continuum of hydrogen.

During the time of flares, the x-ray intensities may be enhanced considerably and may make a greater contribution to the E region electron density. In fact, according to Friedman [48], x-ray intensities as high as 1.0 erg cm^{-2} sec^{-1} have been observed. However, in view of the difficulty in the interpretation of photon counter data [7], it seems desirable to study this spectral region with monochromators.

According to Nicolet and Aikin [1] the dissociative recombination rates for N_2^+ is $5x10^{-7}$ $cm^3 sec^{-1}$ and for O_2 $3x10^{-8}$ cm^3 sec^{-1}. If these rates are approximately correct, the effectiveness of x-ray ionization is reduced because the slower reaction

$$O_2^+ + e \rightarrow O' + O'' \qquad (11)$$

will tend to control the electron density in the lower E region.

As we proceed upward, the relative amount of O^+ ion increases, additional amount of radiation in the region below 911 A becoming available. Following Bates [49], the recombination of O^+ ion may be largely controlled by the reactions.

$$O^+ + O_2 \rightarrow O_3^+ + O \qquad (12)$$

$$O_2^+ + e \rightarrow O' + O'' \qquad (12a)$$

where Eq. 12 tends to become the rate limiting process; on the other hand, N_2^+ recombines rapidly by dissociative recombination.

Our computations show that the base of the E region is controlled mainly by Lyman beta and partly by other radiation in the spectral region 1000-1027 A where N_2 is very transparent. For example, in the case of $Z = 0^{\circ}$, Lyman beta contributes about 80 percent of the total ionization rate at 100 km and about 70 percent at 105 km, so that the electron density curve in the region 95-105 km should closely approximate an ideal Chapman curve. Above this region there is increasing superposition of Chapman-type curves due to several prominent emission lines in the spectral region 900-1000 A. Our results for the lower E region appear to be in harmony with the description by Ratcliffe and Weekes [50] : "The shape of the layer and the way in which its height varies through the day are roughly what would be expected for an equilibrium Chapman layer found in an atmosphere of scale height 8 km, with its peak at a level of 105 km for vertically incident ionizing radiation."

The electron density and effective recombination in the E region will be discussed in Section IX.

VIII. FORMATION OF THE F REGION. A clearer picture of the vertical distribution of electron density has now become available through rocket and satellite measurements. Jackson [51] , for example, has constructed a curve showing a peak in the F_2 region and only a "ledge" in the F_1 region in place of the peak inferred from numerous ground-based radio observations. In the light of the new data, the term F_1 peak should be revised to F_1 ledge.

Early theories [52] of the F layer have usually invoked two different absorption processes to explain the origin of the two F regions; but according to Bradbury's hypothesis [53] both "layers" are produced by the same radiation and the double layer is due to the rapid decrease of recombination coefficient with altitude. Bates [6,37] considers this hypothesis to be essentially correct.

Our study of the various radiation and related cross sections has failed to reveal any photoionization process giving maximum, noontime rate in the F_2 region. As shown in Fig. 2, Lyman gamma is largely absorbed in the F_2 region by N_2 rather than O_2, so its absorption provides negligible amounts of ionization.

The radiation responsible for the ionization in the F_1 and F_2 regions lie in the broad spectral range 100- 911 A, with the 304 A line of He II as the strongest emission line and large contributions from the ionization continua of hydrogen and helium. As shown in Fig. 3, ultraviolet radiation in this range at vertical incidence produces a maximum ionization rate at 150 km; however, it should be emphasized that many wavelengths and several absorption processes are involved.

A further insight into the production of the F_1 ledge and F_2 peak can be obtained with the aid of Fig. 5 which shows the photoionization rates for different zenith angles. At sunrise the maximum ionization rate ϕ is at about 300 km, approximately coinciding with the height of the peak of the nighttime electron density ($\sim 10^5$ cm^{-3}). Hence, during about an hour period around sunrise, there is a

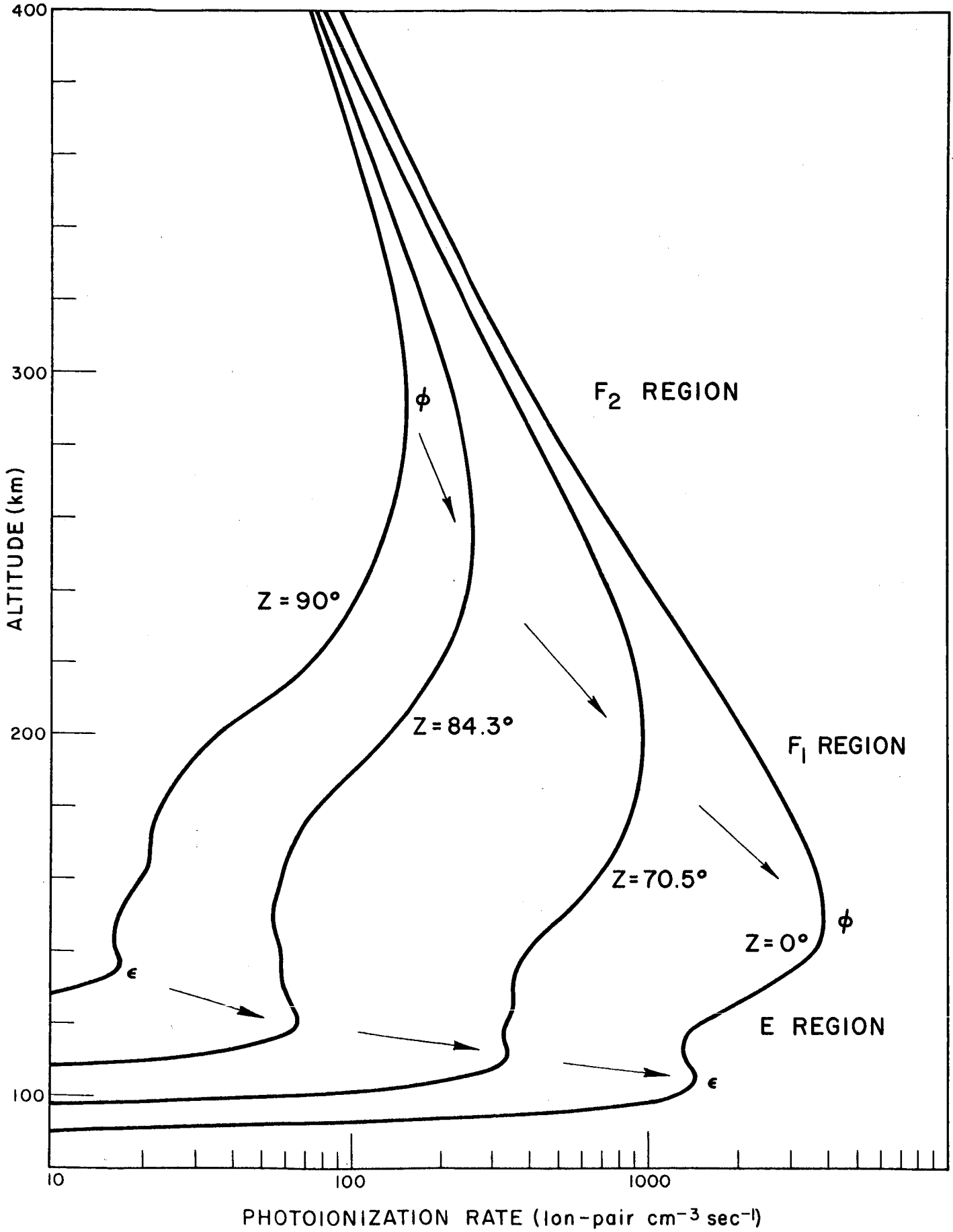

Figure 5. Total Photoionization Rate Versus Altitude for Four Zenith Angles. Arrows show the direction of displacement of the peaks, phi and epsilon.

comparatively high "build up" of electron density at this altitude due to the combined effect of the low recombination rate and relatively high ionization rate. As the sun rises, the location of the maximum ionization rate ϕ descends rather rapidly to the F_1 region, but due to the higher recombination rates found at lower altitudes, the F_2 electron density peak at 300 km or somewhat lower does not correspondingly shift downward; only a ledge appears in the electron density curve and descends to about 150 km. In other work, the so-called "splitting" or "bifurcation" of the F layer is the result of the enhancement and persistence of the F_2 peak and the movement of the F_1 ledge. Thus, our study supports the work of Bradbury [53], Bates [37] and others.

The behavior of the F region ionization is much more complicated than our simple picture may suggest, and no doubt other processes must be included in order to explain the numerous irregularities and anomalies observed by radio techniques.

In the next section we briefly discuss the question: "Are the calculated ionization rates consistent with the observed electron densities?"

IX. ELECTRON DENSITY AND RECOMBINATION COEFFICIENT IN THE E AND F REGIONS. The following equation may be used to estimate the electron density and its variation with time:

$$dn/dt = q - \alpha n^2 \qquad (13)$$

where n = electron density, q = effective electron production rate and

α = effective recombination coefficient. Published values of α show a wide spread; for example, Bates and Massey[54] have used 1×10^{-8} $cm^3 sec^{-1}$ for the E layer (at 120 km) and Mitra and Jones[55] have reported 6×10^{-8} $cm^3 sec^{-1}$ at 100 km and 1.6×10^{-8} $cm^3 sec^{-1}$ at 140 km. The variation of α with altitude is approximately represented by the broken curve in Fig. 6, which shows a rapid decrease of α between 150 and 300 km. In the following paragraphs we attempt to show by Eq. 13 and with assumed values of α that the calculated photoionization rates give electron densities approximately agreeing with observed values.

Near the bottom of the E region at about 105 km, photons in the range 1000-1027 A produce most of the electrons by photoionization of O_2, since the absorption by O and N_2 is negligible. Therefore, q in Eq. 13 is nearly equal to the calculated photoionization rate, p. The effective rate is very small at sunrise but reaches about 100 $cm^{-3} sec^{-1}$ after one-half hour and exceeds 500 $cm^{-3} sec^{-1}$ in 2 hours. By numerical integration and successive approximation, n is found to increase rapidly during the same period so that we have quasi-equilibrium, which permits us to let $dn/dt \sim 0$ in Eq. 13. Using $\alpha = 2.5 \times 10^{-8}$ $cm^3 sec^{-1}$, q = 1400 $cm^{-3} sec^{-1}$ for Z = 0 (see Fig. 5), we obtain $n = 2.4 \times 10^5$ cm^{-3} which is the correct order of magnitude for the maximum electron density in the E region (see solid curve in Fig. 6). It should be added that x-rays produce some N_2^+ and O^+ ions (as well as some O_2^+), the former recombining more rapidly than O_2^+ and the latter more slowly. Ionic composition determined by Johnson et al[56] shows that O_2^+ is much more prevalent than O^+ at this altitude; thus their result tends to support our calculations.

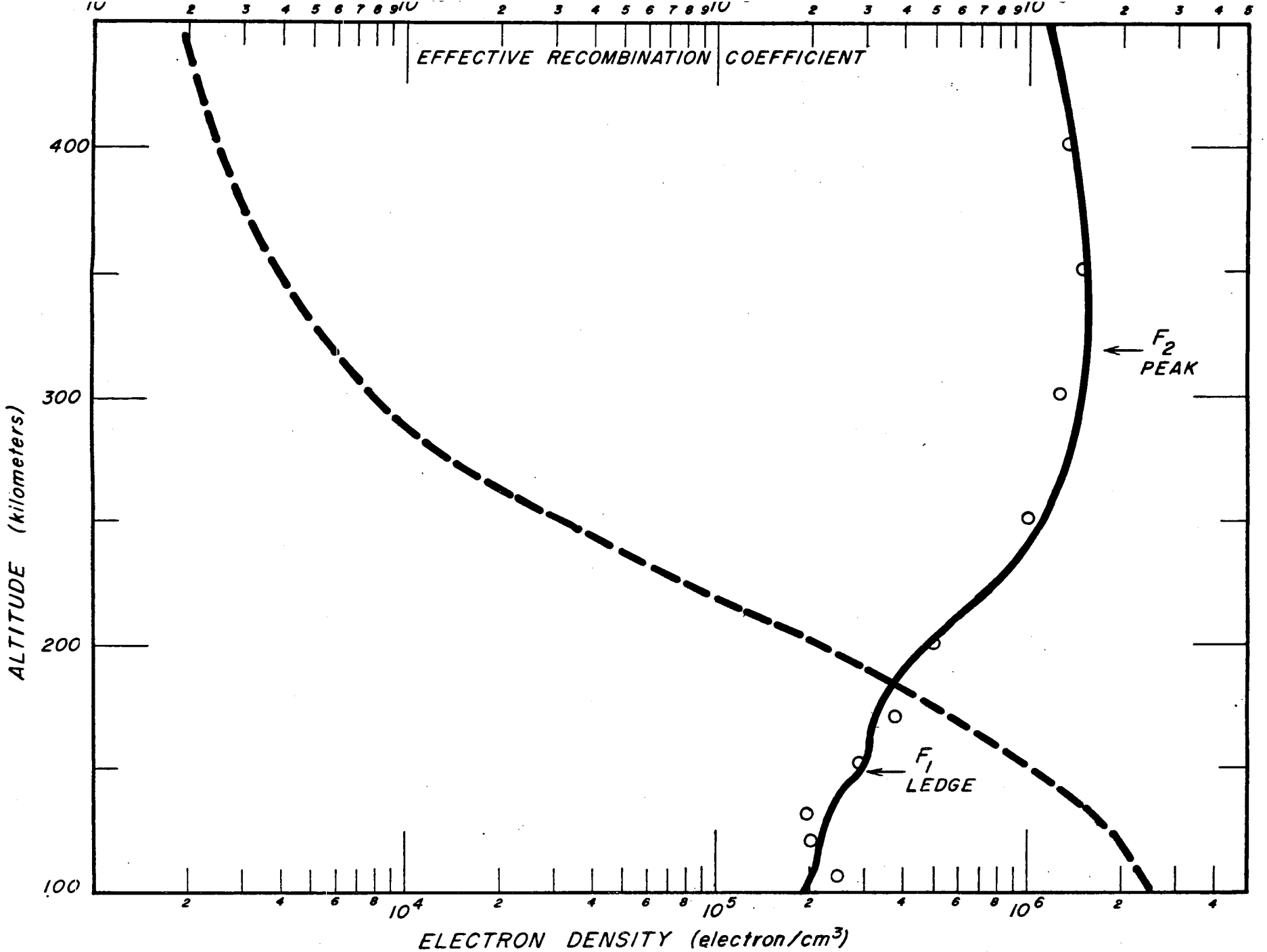

Figure 6. Broken curve represents effective recombination coefficients (in $cm^3 sec^{-1}$) versus altitude. Solid curve represents electron density versus altitude according to Jackson.

Furthermore, the effective recombination coefficient of 2.5×10^{-8} cm^3 sec^{-1} at this altitude appears to be compatible with the process of dissociative recombination of O_2^+.

In the upper E region at about 130 km, the radiation in the region below 911 A as well as radiation in the region 911-1000 A plays an important role, especially for near vertical sun. Photons in these regions can ionize O and N_2 as well as O_2. It is important to note in passing that NO^+ which is the most numerous ion [56] at this altitude may be produced by one or more reactions involving O^+ and N_2^+ discussed by Bates and Nicolet [18]. Since N_2^+ presumably disappears by dissociative recombination faster than the other ions discussed here, we cannot let the calculated photoionization rate (2500 cm^{-3} sec^{-1}) equal q. However, q cannot be obtained directly from p because it is necessary to know the several recombination processes and their rates, as well as the number densities, photoionization cross sections, and the spectral intensity distribution. Tentatively we may assume that N_2^+ recombines so rapidly that the photoionization of N_2 constitutes only a minor contribution to the electron density. Hence, for this altitude we take q equal to about one-fourth of p. This value of q combined with α = 1.7×10^{-8} $cm^3 sec^{-1}$ yields $n = 1.7 \times 10^5 cm^{-3}$ for the noontime electron density. This density is somewhat lower than that for the 105 km level, and it seems possible that there is a shallow minimum in the electron density curve.

Near the bottom of the F_1 region at about 170 km, the nighttime electron density is about 10^4 cm^{-3}, and according to our numerical

integration, this density is increased to 10^5 cm^{-3} at the end of the first hour after sunrise. After this period, we have quasi-equilibrium as in the E region. Taking q equal to about one-fifth the calculated photoionization rate (3500 $cm^{-3}sec^{-1}$) and letting $\alpha = 6\times10^{-9}$ cm^3sec^{-1}, we obtain $n = 3.4\times10^5$ cm^{-3} as the maximum electron density of the F_1 ledge; this value is in line with the electron density curve [51]. The recombination coefficient used here is comparatively high but is consistent with the relatively high O_2 concentration in our model atmosphere (Table 4). In other words, the slower recombination process involving O^+ is not fully effective as the rate determining process.

In the F_2 region at about 300 km, the nighttime observed electron density is about 2×10^5 cm^{-3} and according to our numerical integration, this density is only doubled during the first hour after sunrise and increases rather slowly compared to the situation at lower altitudes. As shown in Fig. 5, the photoionization rate is nearly constant after the initial one hour. If q in Eq. 13 is constant, the electron density is given by the equation

$$n = (q/\alpha)^{\frac{1}{2}} \tanh \left[(\alpha q)^{\frac{1}{2}} t + \text{const.} \right] \qquad (14)$$

and n approaches the limit $(q/\alpha)^{\frac{1}{2}}$. If we let q be one-third of the photoionization rate (the relative amount of N_2 being less here than at lower altitudes) and $\alpha = 8\times10^{-11}$ cm^3sec^{-1}, we obtain $n = 1.3\times10^6$ cm^{-3} as the maximum electron density which compares favorably with observed values.

Table 4. Estimated electron density, n_e, versus altitude (h in km)

h	p	q/p	n_e
95	400	1	1.2×10^5 electron/cm^3
105	1400	1	2.4
120	1500	½	2.0
130	2500	¼	1.9
150	3900	¼	3.0
170	3400	¼	3.8
200	2200	¼	5
250	890	1/3	10
300	380	1/3	13
350	180	½	15
400	92	½	14

Similar estimates of electron density at other altitudes are listed in Table 4 and also shown by points in Fig. 6. The combined uncertainty in our data may be as high as a factor of five, so that the present estimates are only semi-quantitative. However, these values indicate a maximum electron density at about 350 km, a ledge in the electron density curve at about 150 km, a possible minimum at about 130 km, and a lower maximum about 105 km.

X. CONCLUSION. As a summary we briefly list several conclusions which may be drawn from the present study, although some of them must be regarded as tentative.

1. The solar ultraviolet flux used here leads to reasonable photoionization rates; hence, the intensities observed by Hinteregger et al and Tousey et al are probably correct to within a factor of five and possibly a factor of two.

2. Ionization in the E region can be explained by the ultraviolet radiation in the spectral range 900-1027 A. The base of the E region is due to Lyman beta. Soft x-rays make only a small contribution, unless the reported intensity is too low by at least an order of magnitude.

3. Both the F_1 and F_2 regions are produced mainly by radiation in the range 100-900 A and Bradbury's hypothesis is essentially correct. The F_1 ledge can be correlated to the peak of the photoionization rate and the F_2 peak can be ascribed to the combined effect of the low recombination rate and the comparatively high photoionization rate throughout the day at an altitude of about 300 km.

4. The calculated photoionization rates yield quasi-equilibrium electron densities roughly agreeing with observed values in the altitude range 90-400 km.

5. The calculated photoionization rates are consistent with the theory that the recombination rate of the E region is large controlled by the dissociative recombination of O_2^+.

6. The recombination rate in the F_2 region is probably controlled by the recombination of O^+ as proposed by Bates.

7. The greatest uncertainty in our calculation is the composition of the atmosphere above 150 km.

ACKNOWLEDGMENT

We gratefully acknowledge our indebtedness to Drs. H.E. Hinteregger and R. Tousey who provided valuable material on the solar ultraviolet spectrum.

APPENDIX

As mentioned in Section IV, available data on absorption coefficient of O_2 and N_2 are incomplete and there are disagreements. Experimental values at many of the prominent lines are listed in Table 5. For O_2, the available data is fairly satisfactory; a rather dense distribution of absorption coefficient and ionization yield in the region 850-1100 A have been reported by Watanabe and Marmo [24] and k-values at many wavelengths down to 200 A have been determined by Lee [57]. Photoionization yield [24] of O_2 in the region 850-1027 A vary between 50 and 100%, and according to Wainfan et al [58] the yield is similarly high at shorter wavelengths. For the present purpose, the yield may be taken as equal to unity or $\frac{1}{2}$.

For N_2 the uncertainty is somewhat greater especially in the spectral region 800-1000 A. Here, we do not have the ionization continuum as in the case of O_2 and there is a large variation in the k-value. It was found necessary to make estimates from a high dispersion absorption spectrum of N_2 obtained by Ogawa [59] as well as to use new laboratory data obtained by Itamoto et al [25]. For example, the strong Lyman continuum lie throughout the spectral range 850-911 A. Here,absorption coefficients of 10, 100, 500, and 2000 cm^{-1} were used with the following weight distributions: 5%, 45%, 45%, 5%, respectively; this method was considered preferable to the usual method of using a single "mean" coefficient.

For atomic oxygen, the values recommended by Dalgarno[20] were used (see Table 6).

Table 5. Absorption coefficient (k in cm^{-1}) of N_2 and O_2 for some solar ultraviolet emission lines in the region 200-1000 A

λ	N_2	O_2
200	200	300
303.8 He II	160	500
584.3 He I	520	540
609.7 Mg X	?	600
787.7 O IV	250	?
790.2 O IV	670	?
832.7 O III	92	670
833.3 O II	260	380
833.7 O III	230	340
835.3 O III	120	300
903.6 C II	300	250
903.9 C II	25	240
904.5 C II	250	210
937.8 H I	200	115
949.7 H I	90	160
972.5 H I	7600	1000
977.0 C III	100?	90
989.8 N III	?	60
1025.7 H I	0.01	45

Table 6. PHOTOIONIZATION CROSS SECTIONS σ OF ATOMIC OXYGEN IN CM^2 ACCORDING TO DALGARNO

Wavelength (A^o)	σ (cm^2)	Wavelength (A^o)	σ (cm^2)
911	2.6×10^{-18}	153	2.2×10^{-18}
769	3.4×10^{-18}	131	1.5×10^{-18}
732	3.5×10^{-18}	115	1.1×10^{-18}
		100	8.5×10^{-19}
		83	5.3×10^{-19}
		70	31.7×10^{-19}
		52	2.3×10^{-19}
732	7.6×10^{-18}	40	1.2×10^{-19}
665	8.6×10^{-18}	34	9.1×10^{-20}
		30	6.8×10^{-20}
		26	4.1×10^{-20}
		22.8	2.0×10^{-20}
665	1.1×10^{-17}		
587	1.3×10^{-17}		
525	1.3×10^{-17}		
475	1.3×10^{-17}	22.8	5.3×10^{-19}
455	1.1×10^{-17}	20	4.0×10^{-19}
435	9.8×10^{-18}	15	2.0×10^{-19}
		8	3.6×10^{-20}
		6	1.6×10^{-20}
		5	9.5×10^{-21}
		4	5.0×10^{-21}
435	1.3×10^{-17}	3	2.1×10^{-21}
400	1.2×10^{-17}	2.5	1.3×10^{-21}
365	1.0×10^{-17}	2.0	6.7×10^{-22}
315	8.0×10^{-18}	1.5	6.7×10^{-22}
310	7.8×10^{-18}	1.0	8.8×10^{-23}
		0.8	4.7×10^{-23}
		0.6	2.3×10^{-23}
		0.5	1.5×10^{-23}
		0.4	1.0×10^{-23}
310	1.0×10^{-17}	0.3	7.0×10^{-24}
290	9.2×10^{-18}	0.25	5.8×10^{-24}
270	8.0×10^{-18}	0.20	5.0×10^{-24}
245	6.3×10^{-18}	0.15	4.4×10^{-24}
220	5.1×10^{-18}	0.12	4.1×10^{-24}
185	3.4×10^{-18}	0.10	3.8×10^{-24}

REFERENCES

1. M. Nicolet and A.C. Aikin, J. Geophys. Res., 65, 1469 (1960).

2. H.E. Hinteregger, K.R. Damon, L. Heroux, and L.A. Hall, paper presented at the "First International Space Science Symposium", Nice (1960); private communication.

3. M.H. Reese and W.A. Rense, J. Geophys. Res., 64, 1251 (1959); T. Violett and W.A. Rense, Astrophys. J., 130, 954, (1960).

4. R. Tousey, J.C. Purcell, and D.M. Packer, paper presented at the "First International Space Science Symposium," Nice (1960); private communication.

5. R.J. Havens, H. Friedman, and E.O. Hulburt, in "Physics of the Ionosphere," Physical Society, London, p. 237 (1955).

6. D.R. Bates, In "Solar Eclipse and the Ionosphere" Special Suppl. Vol. 6, J. Atmos. Terr. Phys., p. 184 (1956).

7. E.T. Byram, T.A. Chubb, and H. Friedman, J. Geophys. Res., 61, 251 (1956).

8. V.V. Mikhnevich, B.S. Denilin, A.I. Repnev, and V.A. Sokolov, "Iskusstvennye Sputniki Zemli," No. 3, USSR, Acad. Sci. Press, Moscow (1959). See translation in ARS Journal, 30, 407 (1960).

9. K.W. Champion and R.A. Minzner, Planet. Space Sci., 1, 259 (1959).

10. G.F. Schilling and T.E. Sterne, J. Geophys. Res., 64, 1 (1959).

11. J.W. Siry, Planet. Space Sci., 1, 184 (1959).

12. R. Horowitz and H.E. LaGow, J. Geophys. Res., 61, 77 (1956).

13. S. Deb, J. Atmos. Terr. Phys., 2, 309 (1952).

14. T. Sato, J. Geomag. Geoelectricity (Japan) 3, 71 (1953).

15. V.G. Istomin, Doklady Academii Nauk USSR, 129, 81 (1959).

16. M. Nicolet, Annales de Geophys., 15, 1 (1959).

17. E.T. Byram, T.A. Chubb, and H. Friedman, Phys. Rev., 98, 1594 (1955).

18. D.R. Bates and M. Nicolet, J. Atmos. Terr. Phys., 18, 65 (1960).

19. K. Watanabe, "Advances in Geophysics," 5, 153 (1958).

20. A. Dalgarno, Fourth Quarterly Report under Contract NASW-124. Geophysics Corporation of America (1960).

21. S. Kato, J. Geomagn. Geoelectricity (Japan) 4, 153 (1954).

22. J.C. Brandt, Astrophys. J., 130, Astrophy. J., 130, 228 (1959).

23. J.D. Purcell and R. Tousey, In "Physics of the Upper Atmosphere," Ed. by J.A. Ratcliffe, Academic Press, p. 557, (1960).

24. K. Watanabe and F.F. Marmo, J. Chem. Phys., 25, 965 (1956).

25. F. Itamoto, F. Matsunaga, H. McAllister, and K. Watanabe, unpublished material.

26. H. Friedman, see Ref. (23), p. 186.

27. S. Chapman, Proc. Phys. Soc., 43, 26 (1931); 43, 484 (1931).

28. S. Chapman, Proc. Phys. Soc., 51, 93 (1939).

29. S. Chapman, Proc. Phys. Soc., B 67, 717 (1954).

30. M. Nicolet and L. Bossy, Ann. de Geophs., 5, 275 (1949).

31. J.A. Glendhill and M.E. Szendrei, Proc. Phys. Soc., B 63, 427 (1950).

32. F.S. Johnson, J. Geophys. Res., 61, 71 (1956).

33. O.R. Wulf and L.S. Deming, Terr. Mag. Atmos. Elect., 43, 283 (1938).

34. M. Nicolet, Mem. Inst. R. Met. Belgique, 19, 124 (1945).

35. L. Vegard, Geofys. Publ. 12, No. 5 (1938).

36. E.O. Hulburt, Phys. Rev., 53, 344 (1938).

37. D.R. Bates, Proc. Roy. Soc. (London), A196, 562 (1949).

38. M. Nicolet, Ann. de Geophys., 8, 141 (1952).

39. D.C. Choudhury, Phys. Rev., 88, 405 (1952).

40. E.T. Byram, T.A. Chubb, and H. Friedman, Phys. Rev., 92, 1066 (1953).

41. E. Bauer and T.Y. Wu, Phys. Rev., 92, 1101 (1953).

42. K. Rawer and E. Argence, Phys. Rev., 94, 253 (1954).

43. T. Sato, Rep. Ionosphere Res. (Japan), 8, 49 (1954).

44. K. Watanabe, F.F. Marmo and J. Pressman, J. Geophys. Res., 60, 513 (1955).

45. R.E. Houston, J. Atm. Terr. Phys., 12, 225 (1958).

46. H. Kamiyama, Science Rept. Tohoku Univ. (Japan), 11, 98 (1959)

47. See for example, E.V. Appleton, Proc. IRE, 47, 155 (1959).

48. H. Friedman, see Ref. 23, p. 193.

49. D.R. Bates, see Ref. 6, p. 191.

50. J.A. Ratcliffe and K. Weekes, see Ref. 23, p. 417.

51. J.E. Jackson, see Ref. 23, p. 108.

52. S.K. Mitra, "The Upper Atmosphere," second ed. The Asiatic Society, Calcutta (1952).

53. N.E. Bradbury, Terr. Mag. Atmos. Elect., 43, 55 (1938).

54. D.R. Bates and H.S.W. Massey, Proc. Roy. Soc., 187, 261 (1946).

55. A.P. Mitra and R.E. Jones, J. Geophys. Res., 59, 391 (1954).

56. C.Y. Johnson, E.B. Meadows, and J.C. Holmes, J. Geophys. Res., 63, 443 (1958).

57. P. Lee, J. Opt. Soc. Am., 45, 703 (1955).

58. N. Wainfan, W.C. Walker, and G.L. Weissler, Phys. Rev., 99, 542 (1955).

59. M. Ogawa, private communication.